Investigation of the Order-Disorder Rotator Phase Transition in KSiH3 and RbSiH3

THE JOURNAL OF PHYSICAL CHEMISTRY C

Article

pubs.acs.org/JPCC

Investigation of the Order–Disorder Rotator Phase Transition in $KSiH_3$ and $RbSiH_3$

Reji Nedumkandathil,[†] Aleksander Jaworski,[†] Andreas Fischer,[‡] Carin Österberg,[§] Yuan-Chih Lin,[§] Maths Karlsson,[§] Jekabs Grins,[†] Andrew J. Pell,[†] Mattias Edén,[†] and Ulrich Häussermann*[,†]

[†]Department of Materials and Environmental Chemistry, Stockholm University, SE-10691 Stockholm, Sweden

[‡]Department of Physics, Augsburg University, D-86135 Augsburg, Germany

[§]Department of Physics, Chalmers University of Technology, SE-41296 Gothenburg, Sweden

Supporting Information

ABSTRACT: The $\beta-\alpha$ (order–disorder) transition in the silanides $ASiH_3$ (A = K, Rb) was investigated by multiple techniques, including neutron powder diffraction (NPD, on the corresponding deuterides), Raman spectroscopy, heat capacity (C_p), solid-state ^2H NMR spectroscopy, and quasi-elastic neutron scattering (QENS). The crystal structure of α-$ASiH_3$ corresponds to a NaCl-type arrangement of alkali metal ions and randomly oriented, pyramidal, SiH_3^- moieties. At temperatures below 200 K $ASiH_3$ exist as hydrogen-ordered (β) forms. Upon heating the transition occurs at 279(3) and 300(3) K for $RbSiH_3$ and $KSiH_3$, respectively. The transition is accompanied by a large molar volume increase of about 14%. The $C_p(T)$ behavior is characteristic of a rotator phase transition by increasing anomalously above 120 K and displaying a discontinuous drop at the transition temperature. Pronounced anharmonicity above 200 K, mirroring the breakdown of constraints on SiH_3^- rotation, is also seen in the evolution of atomic displacement parameters and the broadening and eventual disappearance of libration modes in the Raman spectra. In α-$ASiH_3$, the SiH_3^- anions undergo rotational diffusion with average relaxation times of 0.2–0.3 ps between successive H jumps. The first-order reconstructive phase transition is characterized by a large hysteresis (20–40 K). ^2H NMR revealed that the α-form can coexist, presumably as 2–4 nm (sub-Bragg) sized domains, with the β-phase below the phase transition temperatures established from C_p measurements. The reorientational mobility of H atoms in undercooled α-phase is reduced, with relaxation times on the order of picoseconds. The occurrence of rotator phases α-$ASiH_3$ near room temperature and the presence of dynamical disorder even in the low-temperature β-phases imply that SiH_3^- ions are only weakly coordinated in an environment of A^+ cations. The orientational flexibility of SiH_3^- can be attributed to the simultaneous presence of a lone pair and (weakly) hydridic hydrogen ligands, leading to an ambidentate coordination behavior toward metal cations.

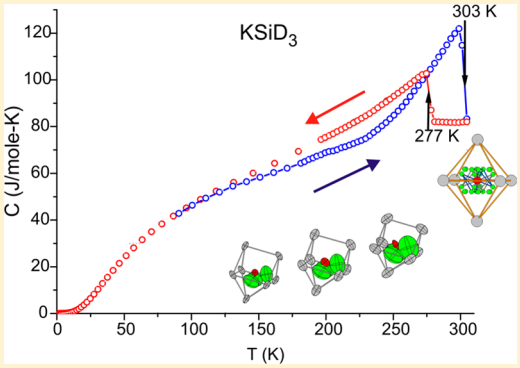

I. INTRODUCTION

Order–disorder transitions in crystals involving rotational dynamics of molecules or complex ions are referred to as rotator phase transitions.[1] Accordingly, rotator phases have a long-range ordered crystal structure with short-range disorder and occur between the low-temperature crystalline phase(s) and the melting temperature.[2] Prominent and classic examples of systems exhibiting rotator phases are H_2, CH_4, P_4, C_{60}, and long-chained *n*-alkanes.[3−7] Typically, rotator phase transitions are associated with anomalies in physical properties, notably the specific heat and the molar volume.[2,8,9] Melting following the rotator state is often associated with an entropy of fusion less than 20 J/(mol K) ("Timmermans rule").[10]

The phenomenon of rotator phase transitions was recognized early; a first comprehensive review dates back to Eucken in 1939.[11] In the beginning (e.g., Pauling in 1930),[12] rotator phase transitions were regarded as onset of free rotation due to the cumulative breakdown of constraints on molecular rotation (i.e., libration modes). Today it is clear that in the rotator state moieties are rarely freely rotating, but rather display variable and complex dynamics.[13−15] Compared with crystals of globular molecules, rotational dynamics in regular salts with simple complex ions occur at higher temperatures (typically several hundred kelvin above RT) because of the stronger electrostatic interactions. Exceptions are ammonium salts and borohydrides—containing the tetrahedral moieties NH_4^+ and BH_4^-—which may display rotator phase behavior below room temperature.[16−18] In some ammonium salts (e.g., $(NH_4^+)_2B_{12}H_{12}^{2-}$) even a pseudo-free rotation of NH_4^+ ions is realized.[19]

Against this background, the silanides $ASiH_3$ (A = K, Rb, Cs) represent an interesting case. Their crystal structure is built

Received: December 22, 2016
Revised: February 10, 2017
Published: February 13, 2017

DOI: 10.1021/acs.jpcc.6b12902
J. Phys. Chem. C 2017, 121, 5241−5252

from trigonal-pyramidal SiH_3^- anions and alkali metal A^+ cations. The high temperature phase (α-$ASiH_3$) corresponds to a NaCl arrangement of alkali metal ions and randomly oriented, pyramidal, SiH_3^- moieties.[20−22] Note that an average NaCl structure is also adopted by the dynamically disordered alkali metal borohydrides ABH_4 (A = Na, K, Rb, Cs) and ammonium halides NH_4X (X = Cl, Br, I). α-$ASiH_3$ forms upon hydrogenating the Zintl phases ASi.[23,24] Investigations of the thermodynamics of the absorption−desorption process $2ASi + 3H_2 = 2ASiH_3$ revealed an unusually small entropy change for A = K, Rb [55−70 J/(K mol (H_2))]. As a consequence, desorption temperatures of 400−410 K are obtained at 0.1 MPa hydrogen pressure, and the conjecture has been made that the phenomenon relates to a high entropy for α-$ASiH_3$.[23] Assuming dynamical disorder, the situation may be likened to a rotator phase, only that consecutive melting (with a small entropy of fusion) would correspond to hydrogen desorption.

From quasi-elastic neutron scattering measurements we recently confirmed the presence of rotational-dynamical disorder in α-$KSiH_3$ and α-$RbSiH_3$. Activation energies are in a range 30−40 meV, which is lower than for borohydrides and most ammonium salts.[25] Compared to the tetrahedral "globular" moieties NH_4^+ and BH_4^-, SiH_3^- however has a lower symmetry and a higher moment of inertia, and the activation of dynamical disorder near room temperature is not necessarily expected. In this paper we elucidate the order−disorder (β−α) phase transition of $KSiH_3$ and $RbSiH_3$ by multiple techniques in order to obtain its comprehensive characterization and further insight into the onset of SiH_3^- dynamics.

II. EXPERIMENTAL DETAILS

Synthesis. All steps of synthesis and sample preparation were performed in an Ar-filled glovebox (H_2O and O_2 levels <0.1 ppm). The Zintl phase precursors KSi and RbSi (ASi) were prepared from stoichiometric amounts of K (Aldrich, 99.9%), Rb (Aldrich, 99.9%), and Si (Chempur, crystalline powder, 99.999%). Si was pressed into pellets and placed alternately with the alkali metal in a tantalum ampule. The ampules were heated inside a silica tube under vacuum at a rate of 5 K/min to 873 K, held for 30 h, and then cooled to room temperature at a rate of 5 K/min. α-$ASiH_3$ was obtained by heating pellets of KSi and RbSi in a corundum crucible in a stainless steel autoclave to 423 and 373 K, respectively, under a pressure of 50 bar of hydrogen for 24 h (H_2 AGA, 99.99999%). The corresponding deuterides α-$ASiD_3$ were prepared accordingly (D_2 AGA, 99.997%) but employing a longer reaction time (5 days). Hydride and deuteride samples were ground in an agate mortar for subsequent investigations. The phase purity of synthesized ASi, $ASiH_3$, and $ASiD_3$ was checked by powder X-ray diffraction. Diffraction patterns were collected on a Panalytical X'PERT PRO diffractometer employing Cu Kα radiation. Because of the air and moisture sensitivity of all materials, they were sealed in 0.3 mm glass capillaries.

Neutron Scattering. Neutron powder diffraction (NPD) data were obtained on the Polaris diffractometer at the ISIS pulsed spallation neutron source, Rutherford Appleton Laboratory, United Kingdom. Data were collected with the backscattering (130−160°), 90° (85−95°), low angle (28−42°), and very low angle (13−15°) detectors, providing a Q range of about 0.5−31 $Å^{-1}$. Samples (approximately 3.4 g of $KSiD_3$ and 4.4 g of $RbSiD_3$) were contained in cylindrical thin-walled 11 mm diameter vanadium cans which were sealed using an indium gasket. The cans were placed in a closed-cycle cryostat, located in front of the backscattering detector. Subsequently, samples were cooled, and diffraction data were collected for 190 μA h at 9 ($KSiD_3$) and 11 ($RbSiD_3$) temperatures over the range of 150−310 K. Data were analyzed using the GSAS refinement software PC-GSAS and EXPGUI.[26,27] Both samples contained small fractions of AD impurity, ∼1.5 and ∼5 wt % for $KSiD_3$ and $RbSiD_3$, respectively. Refinements were performed in the typical sequence, treating first background, then unit cell parameters, atom position parameters, and displacement parameters (temperature factors) U. Peak-shape function 3 was used to model the peak-shapes observed on Polaris.

Quasi-elastic neutron scattering (QENS) experiments were performed at the time-of-flight disk chopper spectrometer (DCS) at the NIST Center for Neutron Research, Gaithersburg (USA). The fine ground materials (approximately 2.5 g of $KSiH_3$ and 2 g of $RbSiH_3$) were thinly distributed inside aluminum foil packets, which were subsequently rolled into 100 mm long annuli with diameters of 17.5 mm. Indium wire sealed aluminum cans were used as sample holders, and cadmium beam masks were used on the top and bottom of the cans. A closed-cycle refrigerator was used to reach the desired temperatures. Measurements were performed using two neutron wavelengths, 2.5 and 4.8 Å. For 2.5 Å neutrons, the energy resolution and accessible Q-range of the spectrometer were 745 μeV full width at half-maximum and 0.98−4.48 $Å^{-1}$, respectively. For 4.8 Å neutrons, the respective values were 110 μeV and 0.52−2.46 $Å^{-1}$. The typical measuring time was between 2 and 4 h. For $KSiH_3$, spectra were measured at 310, 300, 293, 285, 275, 273, 270, 268, 265, 260, 255, 250, and 50 K (in that order, i.e., upon cooling), using both neutron wavelengths. Spectra were also measured upon heating, at 275, 280, 285, 290, 295, 300, 305, and 310 K, with 4.8 Å neutrons. For $RbSiH_3$, spectra were measured at 310, 280, 260, 250, 240, 230, 220, 210, and 50 K (upon cooling), using both neutron wavelengths. Spectra were also measured upon heating, at 240, 255, 270, 285, 300, and 310 K, with 4.8 Å neutrons. Measurements of an empty cell and a vanadium standard, as well as a dark count measurement, were used for the background correction. The spectra measured at 50 K were used as resolution functions in the data analysis. The QENS spectra were reduced and analyzed using the DAVE software.[28]

Heat Capacity Measurements. For heat capacity measurement powders of $ASiH_3$ and $ASiD_3$ were pressed into pellets with 5 mm diameter with masses 8.582, 11.691, 2.777, and 6.463 mg for $KSiH_3$, $KSiD_3$, $RbSiH_3$, and $RbSiD_3$, respectively. The heat capacity was measured between 303 and 2 K (50 points distributed logarithmically and in 3 K steps across the phase transitions from both sides) using a quasi-adiabatic step heating technique as implemented in the Physical Property Measurement System (PPMS) by Quantum Design. Estimated overall heating and cooling rates were on the order of 0.1 K/min. The samples were thermally connected to the platform of the sample holder via small amount of Apiezon-N grease (typically 0.1−0.3 mg). The uncertainty for this measurement technique is generally estimated to be lower than 5%. For the measurements from low to high temperatures below the phase transition, the sample coupling was significantly lower than for the measurements from high to low temperatures for unknown reasons. After passing the phase transition, the sample coupling attained similar values as before. It is therefore possible that the absolute values of the heat

DOI: 10.1021/acs.jpcc.6b12902
J. Phys. Chem. C 2017, 121, 5241−5252

capacity upon heating and below the phase transition may be underestimated.

Raman Spectroscopy. Powder samples of $ASiH_3$ were sealed in 0.3 mm glass capillaries, and Raman spectra were measured on a Dilor XY-800 triple grating spectrometer with double subtractive configuration. The instrument is equipped with an 800 mm focal length spectrograph and a liquid nitrogen cooled, back thinned CCD detector. Capillaries were placed in a Linkam temperature stage and first cooled to 100 K, and spectra were collected at 100, 150, and 200 K. After that a heating−cooling cycle was performed in the interval 200−300 K. At each target temperature samples were equilibrated for 10 min. Samples were excited with a Ar^+/Kr^+ laser (647 nm) with the input power of the laser locked at 10 mW, which approximately corresponds to 0.90 mW output power under the microscope with the ×50 objective lens. Data covering the range 50−400 cm^{-1} were collected in a single spectral window using an 1800 grooves/mm grating. The exposure time was 90 s, and each spectrum comprised five accumulations.

Solid-State NMR Spectroscopy. The NMR experiments were performed on powders of $RbSiD_3$ and $KSiD_3$, which were packed into 3.2 mm zirconia rotors. Static ^2H (spin I = 1) NMR spectra were collected at a magnetic field of 14.1 T with a Bruker Avance-III spectrometer (−92.1 MHz Larmor frequency). The NMR acquisitions involved 4.0 μs radio-frequency pulse at a nutation frequency of 62 kHz. Between 32 and 128 signal transients with 120 s recycle delays were accumulated for each spectrum. Neat, deuterated tetramethylsilane (TMS-d_{12}) was used for ^2H chemical shift referencing. ^2H NMR spectra were recorded upon cooling in the temperature range from 300 to 200 at 10 K intervals. A measurement was also performed on $KSiD_3$ at 290 K upon heating from 200 K. Before starting each final acquisition, the sample was held for 30 min to equilibrate after reaching the desired temperature (stabilized within ±0.1 K). A powder of $Pb(NO_3)_2$ was used for the temperature calibration.[29]

III. RESULTS AND DISCUSSION

Structural Relationship between α- and β-$ASiH_3$. The hydrogenation of RbSi and KSi at elevated temperatures (373−423 K) affords roentgenographically pure samples of α-$ASiH_3$ with an average cubic NaCl type structure in which pyramidal SiH_3^- units with C_{3v} symmetry are orientationally disordered. At temperatures below 200 K $ASiH_3$ exist as hydrogen-ordered β-phases.[22,24] Tang et al. established the structures of β-$KSiH_3$ and β-$RbSiH_3$ from neutron powder diffraction data of $ASiD_3$ measured at 1.5 K.[24] β-$KSiH_3$ crystallizes with an orthorhombic *Pnma* structure whereas β-$RbSiH_3$ adopts the monoclinic $P2_1/m$ $KClO_3$ structure. In both structures, silyl groups possess a local C_s symmetry, but their geometry deviates only slightly from C_{3v}. The average Si−H bond length in the β-phases is 1.54 Å, whereas it is 1.52 Å in the disordered α-forms.[30]

The structures of high-temperature α-$KSiH_3$ and low-temperature β-$KSiH_3$ are compared in Figure 1. A relationship between both structures becomes most apparent when considering a plane {110} in the NaCl structure. Such a plane is shown in Figure 1a where rows of nearest-neighbor coordinated atoms/ions run parallel along the cubic unit cell axis directions. Corresponding planes in the orthorhombic β-phase structure are the (mirror) planes (0,y,0), y = 1/4, 3/4, also shown in Figure 1a. Instead of straight rows, ions are arranged as zigzag chains, yielding a hexagon pattern with mutually 3-coordinated ions. The different arrangement of ions

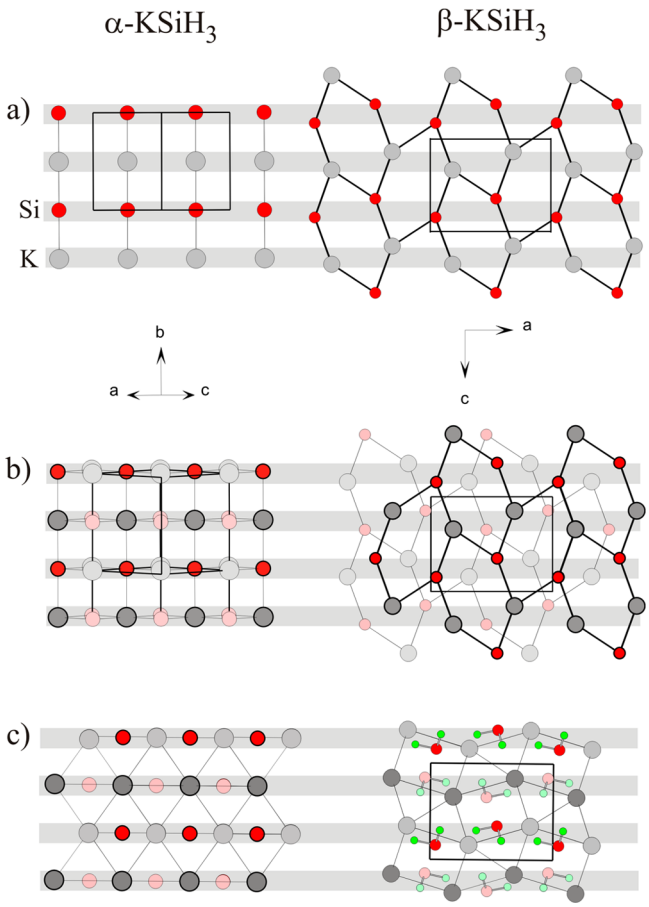

Figure 1. Comparison of the crystal structure of cubic α-$KSiH_3$ (left panel) and orthorhombic β-$KSiH_3$ (right panel). (a) {110} plane in the NaCl structure (left) and corresponding plane (0,1/4,0) in the β-$KSiH_3$ structure (right). Gray circles represent K cations and red circles SiH_3^- moieties. Gray bars mark corresponding rows of ions in both structures. (b) Stacking of {110} planes in the NaCl structure (left) and (0,y,0), y = 1/4, 3/4 planes in the β-$KSiH_3$ structure (right). Dark and light colors differentiate atoms on different heights. (c) Same as (b), but drawn lines are now emphasizing polyhedra around anions, i.e., octahedra for the NaCl structure (left) and monocapped trigonal prisms for β-$KSiH_3$ (right, H atoms are depicted as green circles).

in these planes represents actually the major difference between the two structures. The NaCl structure (α-phase) is completed by stacking {110} planes with a spacing of $a/\sqrt{2}$ (Figure 1b). Atoms achieve their mutual 6-coordination by two additional nearest neighbors situated in each plane adjacent a central one in the stack. The β-phase structure is completed exactly the same way. The stacking of layers occurs in the b direction with a spacing of $b/2$. This results in a mutual 7-coordination of ions. The increased coordination with respect to the NaCl structure is then due to the 3-coordination of ions within a single plane. Figure 1c depicts the same projection as Figures 1a,b, but emphasizing the coordination of Si/SiH_3^-.

The actual local coordination of Si/SiH_3^- in both structures is then shown in Figure 2. The polyhedron defined by the 7 K^+ cations encapsulating SiH_3^- in β-$KSiH_3$ corresponds to a monocapped trigonal prism (Figure 2a). Each H ligand is coordinated by three K^+ ions which results in a quasi-tetrahedral environment. H coordination involves six K^+ ions around a Si atom; the three $HSiK_3$ tetrahedra share common edges. The seventh K^+ ion around a Si atom is situated on the

DOI: 10.1021/acs.jpcc.6b12902
J. Phys. Chem. C 2017, 121, 5241−5252

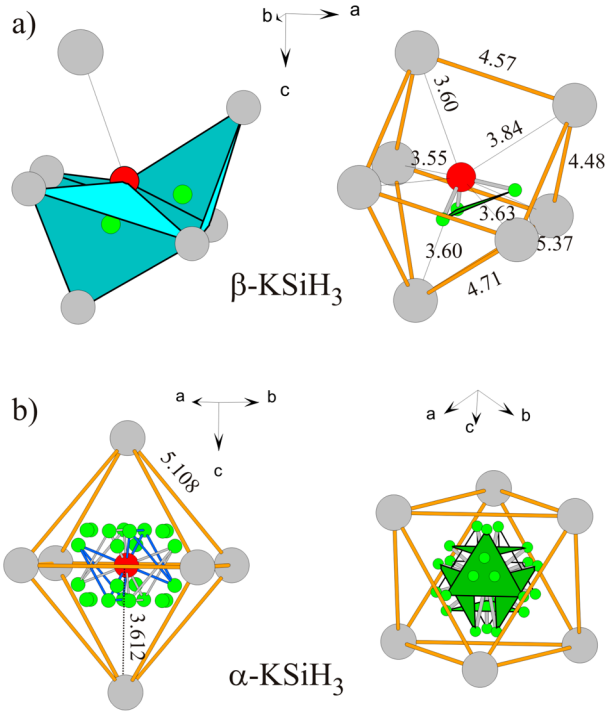

Figure 2. (a) Two views of the monocapped trigonal prismatic coordination environment of SiH_3^- ions in the β-$KSiH_3$ structure. H ligands are coordinated by three K ions each. The resulting $HSiK_3$ tetrahedra share edges (left). (b) Two views of the octahedral coordination environment of SiH_3 ions in the α-$KSiH_3$ (and α-$RbSiH_3$) structure. Pyramidal SiH_3 ions are randomly aligned along the C_3 axes of the K_6 octahedron, coinciding with the directions of the four body diagonals of the cubic unit cell. Orientations of SiH_3^- ions are indicated by blue and gray lines (left) and green triangles (right), connecting H atoms that belong to a particular moiety. Interatomic K−Si and K−K distances are indicated in Å.

pseudo-3-fold axis of the anion, coordinating its "lone pair" site. The monocapped trigonal prism formed by the alkali metal ions is also the building block of the monoclinic β-$RbSiH_3$ structure; that is, the crystal symmetry lowering does not affect the local symmetry of the silyl anions and their coordination by counter cations. The difference between the orthorhombic β-$KSiH_3$ and monoclinic β-$RbSiH_3$ structure is a different linking of these monocapped trigonal prisms. This is shown in the Supporting Information, Figure S1.

In α-$ASiH_3$ dynamically disordered SiH_3^- moieties are surrounded octahedrally by six A^+ ions (Figure 2b). Although the coordination number is larger in β-$KSiH_3$, the average K−Si distance (2×3.55, 2×3.60, 2×3.63, 3.84 Å) is comparable to the one in α-$KSiH_3$ (6×3.61 Å), which implies that the A−A distances in α-$ASiH_3$ are considerably larger than in β-$ASiH_3$. Crystallographically, disordered SiH_3^- expresses itself by a weakly occupied site 96k in the $Fm\bar{3}m$ NaCl structure.[23,24] This renders a truncated-cube-shaped environment of 24 H atom positions (occupied at a 12.5% level) around each Si (cf. Figure 2b). The average crystallographic structure of disordered $ASiH_3$ is based on eight (random) orientations for each SiH_3^- ion. These orientations correspond to alignments (both "up" and "down") of pyramidal SiH_3^- ions (with respect to their C_3 axis) along the directions of the four body diagonals of the cubic unit cell. According to QENS, these 24 positions represent jump locations of H atoms which are associated with the rotational diffusion mechanism of SiH_3^- ions.[25]

β–α Phase Transition Probed by NPD and Raman Spectroscopy. Figure 3 shows the evolution of diffraction patterns with temperature, from 150 K across the phase transition. The 150 K patterns can be fit to the structure models established by Tang et al. from 1.5 K data.[24] For $KSiD_3$ the orthorhombic β-$KSiH_3$ structure is maintained until the phase transition, which occurs between 300 and 310 K. Reflections of the β-phase are, however, still present in the 310 K pattern. For $RbSiD_3$ deviations from the original monoclinic structure are observed with increasing temperature. For patterns above 240 K a triclinically distorted structure provides a better fit. In the pattern obtained at 278 K the α-phase emerges. The pattern at 296 K corresponds then to the pure α-phase (for details, see Supporting Information, parts 2 and 3).

The change of the molar volume in the interval 150−310 K is shown in Figure 4. For $KSiD_3$ there is roughly a linear dependence until the phase transition and a drastic increase at the phase transition by 14%. The situation is similar for $RbSiD_3$. The triclinic distortion manifests itself in irregular molar

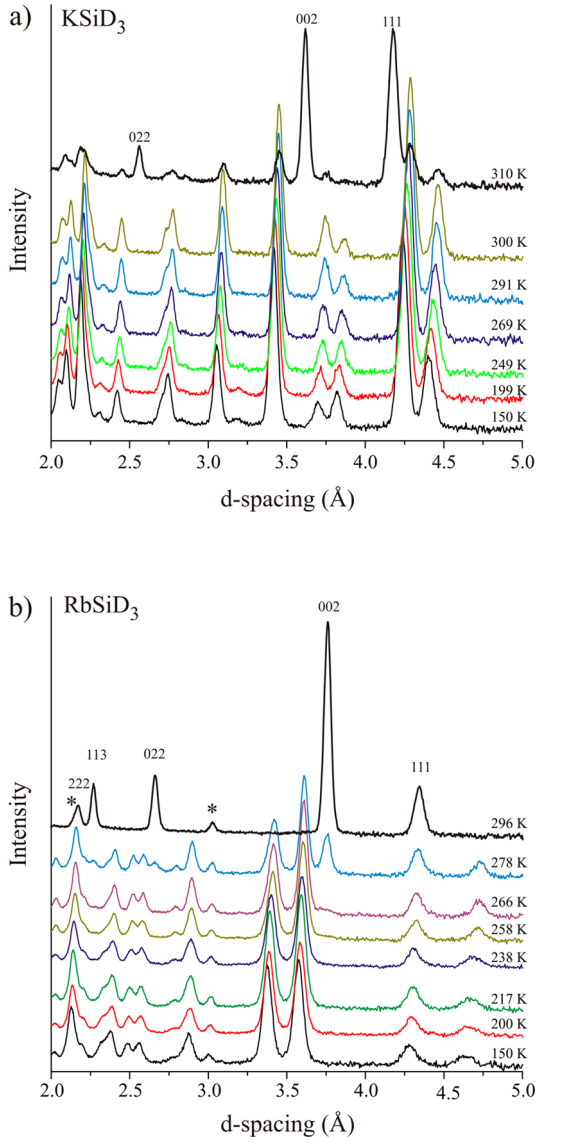

Figure 3. Evolution of NPD patterns of $KSiD_3$ (a) and $RbSiD_3$ (b) when heating from 150 to 310 K. The asterisks mark reflections of RbD impurity. Indices refer to reflections of α-$ASiD_3$.

DOI: 10.1021/acs.jpcc.6b12902
J. Phys. Chem. C 2017, 121, 5241−5252

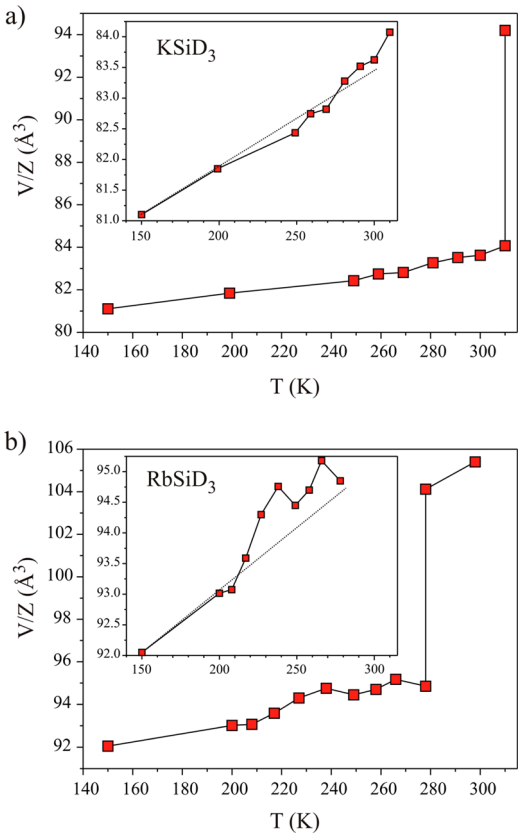

Figure 4. Evolution of molar volumes (V/Z) for $KSiD_3$ (a) and $RbSiD_3$ (b) from 150 to 310 K. See Supporting Information, parts 2 and 3, for details.

volume variations above 240 K. We note that the increase of molar volume across the β-to-α phase transition is enormous. Increases of this magnitude are rarely observed in order−disorder transitions of inorganic materials and actually relate more to the density changes of salts upon melting.[31] Order−disorder transitions of borohydrides and ammonium salts are typically accompanied by molar volume changes around 5%,[32−37] with the exception of the CsCl-to-NaCl type transition in NH_4X.[35−37] Disordered NaCl-type NH_4X (called phase I or α-phase in the literature) precedes melting. As a matter of fact, the order−disorder transition of $ASiH_3$ bears resemblance to the CsCl-to-NaCl type transition of NH_4X.

Figure 5 illustrates the strongly anharmonic behavior of β-$ASiD_3$ above 150 K by showing the isotropic atomic displacement parameters (ADPs) as a function of T as obtained from the diffraction studies. A harmonic system above the Debye temperature would display a linear increase. Interestingly for $KSiD_3$ it is one kind of D atoms (D1) showing the most pronounced deviation/anharmonicity (Figure 5a). The evolution of the anisotropic ADPs reveals an anharmonic behavior above 250 K also for Si and K. For $RbSiD_3$ (Figure 5b) trends are obscured by the change in crystal symmetry. It appears that Si attains considerable higher ADP values compared to $KSiD_3$. For both systems ADPs become anomalously large in the dynamically disordered α-phase.

Figure 6 shows the evolution of translation and libration modes as observed from Raman spectroscopy across the phase transition. The vibrational spectrum of β-$ASiH_3$ was analyzed previously.[30,38] SiH_3^- librations are between 300 and 450 cm^{-1} and 270 and 400 cm^{-1} for A = K and Rb, respectively. SiH_3^-

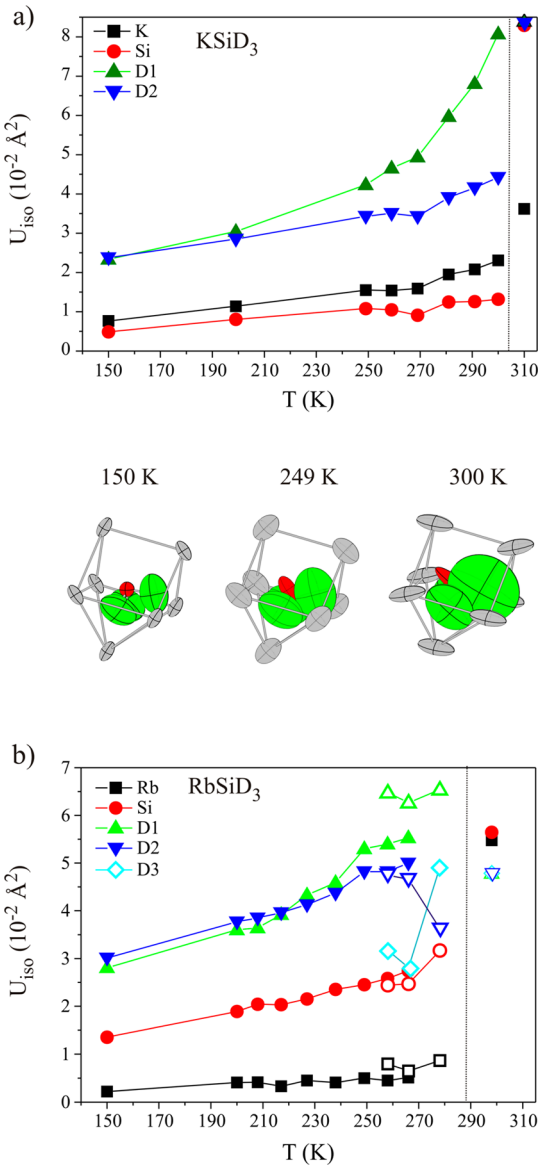

Figure 5. Isotropic atomic displacement parameters (ADPs) U_{iso} as a function of temperature for $KSiD_3$ (a) and $RbSiD_3$ (b). In addition, at the bottom of (a) anisotropic ADPs for β-$KSiH_3$ at 150, 249, and 300 K are displayed. Thermal ellipsoids correspond to a 5% probability density. Open symbols in (b) refer to the triclinically distorted intermediate phase β'-$RbSiD_3$. See Supporting Information, part 3, for details.

translations are between 95 and 160 cm^{-1}, K^+ translations are in the range 60−100 cm^{-1}, and Rb^+ translations in the range 50−70 cm^{-1}. At 100 K the spectra of both compounds display sharp bands for translations and broad bands for librations, which signals a significant anharmonicity for the libration modes already at low temperatures. The libration bands are visible up to 200−220 K; at higher temperatures they are merged into a very broad hump and barely noticeable. At the same time also K^+ and SiH_3^- translation bands broaden significantly but retain the initial shape until their abrupt disappearance at the transition to the cubic α-phase. For $RbSiH_3$, Rb^+ and SiH_3^- translation bands behave differently with increasing temperature. It is clearly seen that anharmonic broadening is much more pronounced for the latter ones. As a matter of fact, SiH_3^- translation bands merge into a broad hump above 220 K

DOI: 10.1021/acs.jpcc.6b12902
J. Phys. Chem. C 2017, 121, 5241−5252

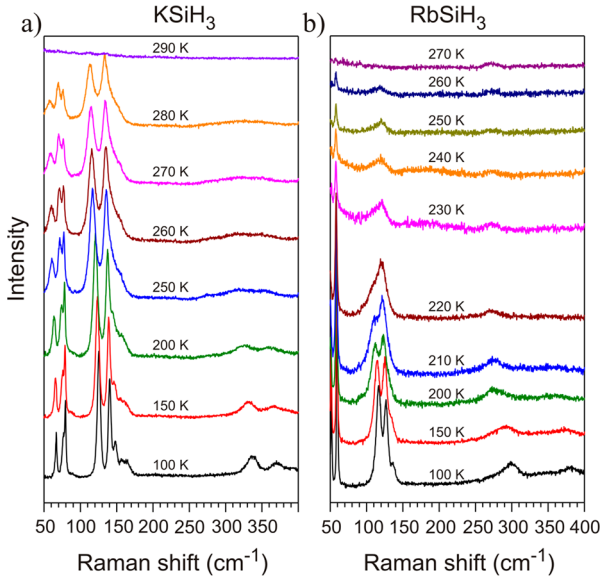

Figure 6. Evolution of Raman spectra of $KSiH_3$ (a) and $RbSiH_3$ (b) when heating from 100 K. The depicted spectral range contains libration bands above 250 cm^{-1}, SiH_3^- translation bands between 95 and 160 cm^{-1}, and A^+ translation bands below 90 cm^{-1}.

whereas Rb^+ translations remain comparatively sharp. This most likely correlates with the transition into the triclinic intermediate. In the Raman study the phase transition to α-$ASiH_3$ is seen at temperatures about 20 K lower compared to the NPD study, which is attributed to a laser-induced local heating of the sample.

To conclude, the NPD and Raman studies revealed a pronounced anharmonic thermal behavior for β-$ASiD_3$/β-$ASiH_3$. This indicates the onset, and even presence, of dynamical disorder already in the low-temperature forms. Indeed, a recent fixed-window scan (FWS) neutron scattering investigation showed that $RbSiH_3$ and $KSiH_3$ start exhibiting dynamics with jump frequencies on the order of 10^8 jumps/s at 150 and 225 K, respectively.[39] This should coincide with a breakdown of librations; that is, torsional oscillations lose translational correlation and SiH_3^- moieties start undergoing independent torsional dynamics on the time scale probed in the FWS experiment (10^8–10^{10} jumps/s). The nature of this dynamics should relate to wagging, perhaps even tumbling, around the axes defining the moments of inertia (i.e., along the C_3 rotational axis (I_A) and two equivalent axes perpendicular ($I_B = I_C$)). Note that the associated mobility is several orders of magnitude lower compared to the rapid (subpicoseconds) dynamics of SiH_3^- in 15% expanded α-$ASiH_3$. Interestingly, the FWS experiments reported in ref 39 show a plateau in scattering intensity for $RbSiH_3$ above 240–250 K until to the phase transition to α-$RbSiH_3$. This plateau, which is absent for $KSiH_3$, possibly refers to the intermediate (triclinic) state in which SiH_3^- ions attain jump frequencies of $\sim 10^{10}$ jumps/s. Next we investigate how the presence of anharmonicity and dynamics in β-$ASiH_3$, and the consecutive phase transition to the rotator α-phase express in heat capacity measurements.

Heat Capacity Variations. Figure 7 compares the heat capacities, C_p, of $ASiH_3$ (see Supporting Information, Figure S2, for $ASiD_3$). There are 15 degrees of freedom associated with a formula unit; 6 correspond to internal modes and 3 each to librations, translations, and the acoustic modes. Accordingly, the Dulong–Petit limit is expected at 125 J/(mol K). Internal

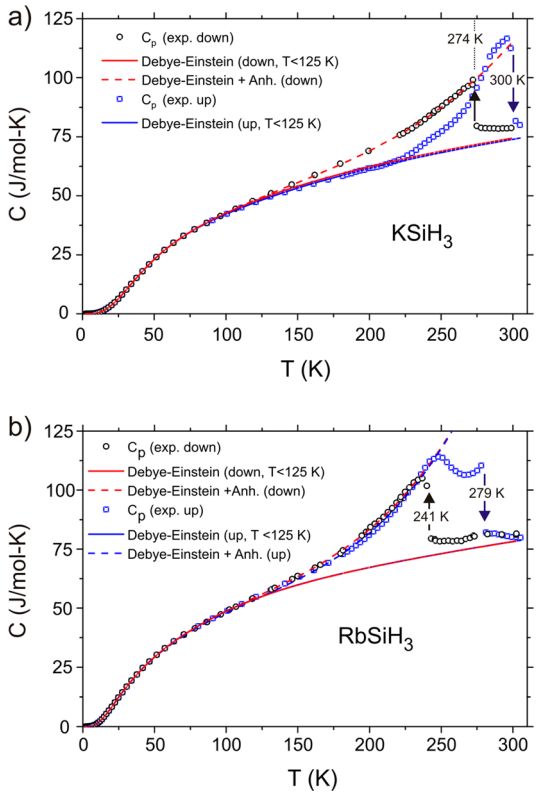

Figure 7. Temperature-dependent heat capacity $C_p(T)$ (per formula unit) of $KSiH_3$ (a) and $RbSiH_3$ (b), one cooling and heating cycle. See Supporting Information, Figure S2, for $C_p(T)$ of $ASiD_3$ and part 4 for details on fitting the data.

modes are observed in the wavenumber ranges 900–1000 cm^{-1} (bending) and 1800–1900 cm^{-1} (stretching)[30] and, thus, will not contribute significantly to $C_p(T)$ up to room temperature. As discussed above, librations are found in a range 300–400 cm^{-1} and translations are around 100 cm^{-1}. At low T it is expected that the $C_p(T)$ behavior corresponds to that of a regular salt, accounted for by translations of A^+ and SiH_3^- ions. To evaluate the $C_p(T)$ data, we used the same strategy that has been previously applied for NH_4X salts.[40,41] The low-temperature data were modeled by a superposition of one Debye and three Einstein terms (i.e., two translations and one rotation), according to the following equations:

$$C_v(T) = 3R(D(T, \Theta_D) + \sum_{i=1}^{k} c_i E_i(T, \Theta_{E,i}))$$

$$C_v(\infty) = 3nR$$

and

$$C_p(T) = C_v(T)(1 + \tilde{C}_v(T)A_1T) \qquad \tilde{C}_v(T) = \frac{C_v(T)}{C_v(\infty)}$$

The thermal expansion was estimated from the unit cell volumes at 1.5 K (as reported by Tang et al.)[24] and at 150 K (our measurements). The fit parameters are provided as Supporting Information (part 4, Table S2). As seen in Figure 7, the so-modeled molar heat capacity agrees well with the measured values at low temperatures. Deviations become noticeable above 130 K and develop subsequently into a pronounced anomaly. Whereas the deviations in the range 130–180 K are a consequence of anharmonicity, affecting the

DOI: 10.1021/acs.jpcc.6b12902
J. Phys. Chem. C 2017, 121, 5241–5252

libration and SiH_3^- translation modes (cf. Figure 6), the anomalous rise of C_p above 200 K is attributed to the onset of dynamical disorder in β-$ASiH_3$. For $RbSiH_3$ another anomaly is seen at around 250 K when C_p slightly drops again. This is attributed to the transition into the intermediate (triclinic) form. We attempted to model the anomalous rise of $C_p(T)$ above 180 K by including empirical anharmonicity parameters in the Debye–Einstein fitting procedure (the formula is given in the Supporting Information). Such parameters are typically used to describe anharmonicity contributions at high temperatures and close to the melting point.[42]

Upon heating the phase transition is observed at 300(3) and 279(3) K for A = K and Rb, respectively. These values are in good agreement with the diffraction studies on the deuterides (above) and the differential scanning calorimetry study by Chotard et al. and Tang et al.[23,24] The phase transition is accompanied by a large drop of C_p (by 30 J/(mol K), or 1.2 R) which for disordered α-$ASiH_3$ then attains a value of about 80 J/(mol K). We note that this behavior is very similar to the CsCl-to-NaCl transition of salts NH_4X,[43] especially $NH_4Br_{0.55}Cl_{0.45}$[44,45] and NH_4I.[46] During this transition, tetrahedral NH_4^+ ions change dynamics from alternating between two orientations (related by a 90° rotation about their C_2 axes) in the CsCl structure into a pseudofree rotation in the NaCl structure.[47,48]

After the phase transition $C_p(T)$ remains almost constant, in agreement with a crystal that either lost its libration modes (that is, turned into a rotator phase) or has its libration modes fully excited (that is, reached the Dulong–Petit limit with respect to the external modes). In each case, $C_p(T)$ will remain flat until the excitation of internal modes. The difference between these two cases represents the "rotational" contribution to C_p.[16] In principle, for an idealized system the transition from a three-dimensional harmonic oscillator (librations) to a free rotor should be accompanied by a loss of 1.5 R and deviations may yield information on the actual rotational dynamics. Such analyses have been attempted for ammonium salts.[43−46,49] In practice, however, it is very difficult to quantify a "rotational" contribution to C_p because of the large uncertainties in describing properly $[C_p - C_v]$, anharmonicity, etc. Nevertheless, from QENS studies it is known that the dynamics of SiH_3^- in α-$ASiH_3$ is not completely "free" but corresponds to a composite mechanism comprising both rotational jumps of H atoms around the C_3 axis of the moiety and jumps related to the 8-fold reorientations of the moiety along the body diagonals of the cubic unit cell, yielding 24 jump locations (cf. Figure 2b).[25]

Hysteresis and Coexistence of α- and β-$ASiH_3$ at Low Temperatures. The order–disorder (β–α) transition in $ASiH_3$ displays a significant hysteresis. Upon cooling, transitions in the C_p measurements are observed at 274(3) and 241(3) K for $KSiH_3$ and $RbSiH_3$, respectively (that is, 26 and 38 K lower, respectively). This has also been observed in previous differential scanning calorimetry experiments.[23,24] The size of the hysteresis is virtually identical for the deuteride analogues, for which transitions are slightly shifted to higher temperatures (by 2–3 K, see Supporting Information Figure S2). It is clear that the α–β transition is reconstructive (cf. Figure 1) and, thus, will proceed by a nucleation-and-growth mechanism. The phenomenon of hysteresis has to be attributed to a lack of equilibrium in the phase transition.[50] It is also noticeable that in the C_p measurements values upon heating and cooling coincide reproducibly only at temperatures considerably below the lower transition temperature (see also Supporting Information, Figure S2, for the deuterides). This could be due to problems with the sample coupling, as mentioned in the Experimental Details section, but it might also indicate the presence of nonequilibrium situations at temperatures below the hysteresis region. To investigate this issue further, we performed solid-state ^2H NMR experiments and evaluated QENS spectra at low temperatures.

In solid-state ^2H (spin I = 1) NMR spectroscopy, the resonances are broadened by the quadrupolar interaction, which is characterized by the quadrupolar coupling constant, $C_Q = e^2qQ/h$, where eQ and eq are the nuclear quadrupolar moment and the largest component ($V_{zz} = eq$) of the electric field gradient (EFG) tensor, respectively. Molecular dynamics will partially, or fully, average the quadrupolar interaction to give an "*effective*" C_Q value, which translates into a narrowed NMR peak-shape.[51,52] Figure 8 shows ^2H NMR spectra collected from static powders of $ASiD_3$ upon cooling from

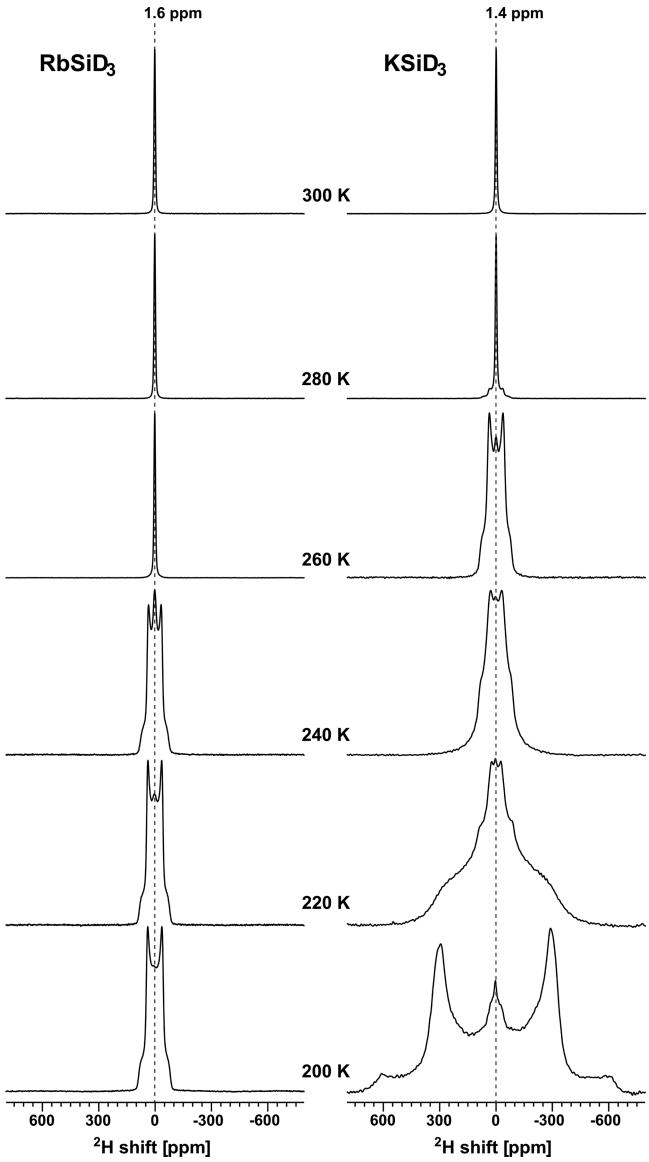

Figure 8. ^2H NMR spectra recorded from static powders of $RbSiD_3$ (left panel) and $KSiD_3$ (right panel) recorded at the as-indicated temperatures on cooling from 300 to 200 K.

DOI: 10.1021/acs.jpcc.6b12902
J. Phys. Chem. C 2017, 121, 5241−5252

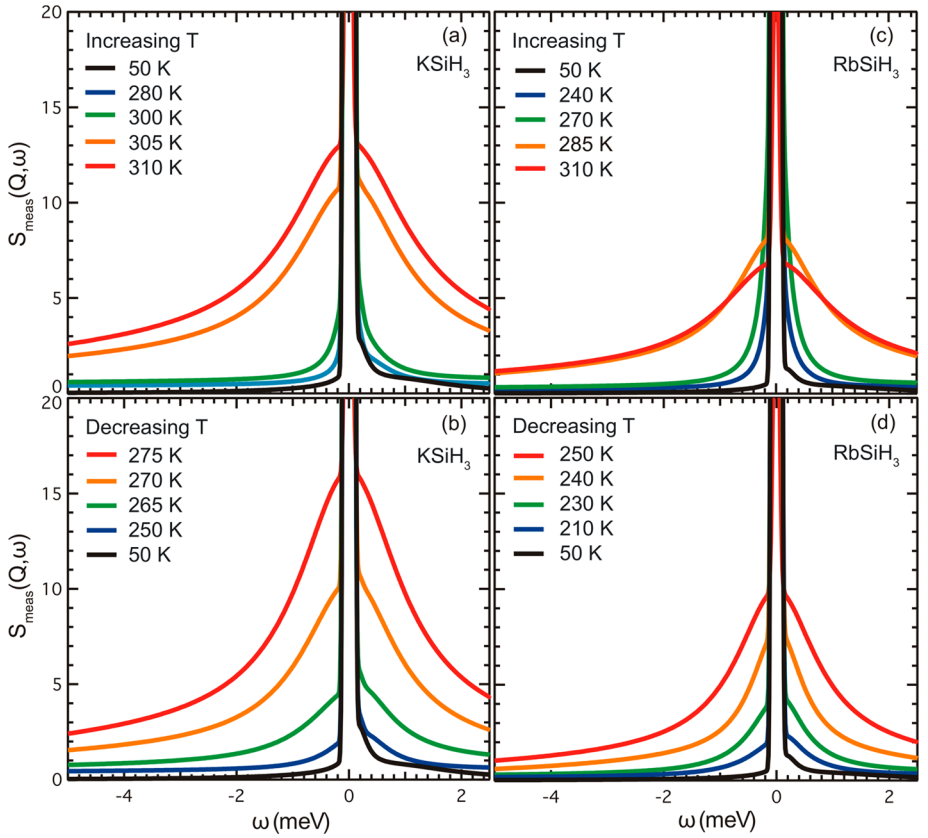

Figure 9. Temperature dependence of the fit to the QENS spectra for $KSiH_3$ (a, b) and for $RbSiH_3$ (c, d) at $Q = 1.9$ Å^{-1}, measured with 4.8 Å neutrons. See Supporting Information, part 5, for details.

300 to 200 K. At 300 K, the presence of rapid dynamics of the SiD_3^- moieties produces one narrow resonance around 1.5 ppm for both α-phases, with a full width at half-maximum (fwhm) height of around 8 ppm. This verifies a complete averaging of the ^{2}H quadrupolar interaction to zero, with the residual peak-width being dictated predominantly by spin−spin (T_2) NMR relaxation. Rapid rotational diffusion with correlation times on the order of 0.2−0.3 ps (as established from QENS)[25] does not contribute effectively to the spin−lattice relaxation times (T_1), which is reflected by the observed relatively long T_1 values (~35 s) for α-$ASiD_3$. When the systems are cooled below the phase transition temperature (260 K for $KSiD_3$ and 240 K for $RbSiD_3$), the NMR spectra manifest the characteristic feature of a quadrupolar-broadened peak-shape, whose width is proportional to the quadrupolar coupling constant.

The presence of (slower) dynamics in the β-phases is then evident from the very low *effective* C_Q values of 10 ± 0.5 kHz for both the β-$RbSiD_3$ and β-$KSiD_3$ phases, as obtained from numerical fitting. Compared to α-$ASiD_3$, T_1 relaxation times are much shorter (<1 s). Upon further cooling of β-$KSiD_3$, the value of C_Q increases to 72 ± 0.5 kHz at 200 K, which indicates that the SiD_3^- motion becomes essentially arrested at this temperature. The dynamical processes only have an effect on the ^{2}H NMR line-shape if the correlation times τ_c associated with them are shorter than the inverse of the first-order quadrupolar interaction frequency in the absence of molecular motions. This would correspond to $\tau_c < 9$ μs, if it is assumed that the motionless limit is at 200 K for β-$KSiD_3$. Therefore, the progressive broadening of the β-$KSiD_3$ NMR peak-shape observed when the temperatures decreases from 240 to 200 K can be attributed to an exchange process with an observed slow motion limit in the microsecond range. The reduction of the slow-motion correlation time is reflected in increasing T_1 relaxation time constants (~30 s) on cooling. We expect the same phenomenon to occur for β-$RbSiD_3$ below 200 K, in agreement with the predictions from the FWS experiments, i.e., the freezing out of dynamics below 150 and 225 K for β-$RbSiD_3$ and β-$KSiD_3$, respectively.[39] However, the correlation times for β-phase dynamics estimated from FWS experiments are on the order of nanoseconds.

The NMR spectra in Figure 8 reveal another important finding, namely, the presence of α-phase well below the phase transition upon cooling. From NMR spectra deconvolutions (not shown), the amount of α-phase observed at 240 K for $RbSiD_3$ and 270 K for $KSiD_3$ is 20% and 3%, respectively. These values drop to 7% and 2% at 220 K ($RbSiD_3$) and 250 K ($KSiD_3$). Small fractions (~1%) of α-phase seem to persist for both systems down to 200 K. This indicates that the nonequilibrium behavior between α- and β-phase extends beyond the range of hysteresis. We speculate that the transformation kinetics α-to-β and/or the relative stability (Gibbs energy difference, ΔG) between the polymorphs depend on the size of α-phase domains. That is, β-phase domains grow at the expense of α-phase during the reconstructive phase transition until α-phase domains obtain a critical size below which the transformation kinetics are considerably slower, or alternatively, G is decreased relative to the β-phase. As a consequence, the α-phase can appear substantially undercooled and a complete transformation will only occur after prolonged annealing at low T. The conjecture of a changed relative stability is supported by an NMR

DOI: 10.1021/acs.jpcc.6b12902
J. Phys. Chem. C 2017, 121, 5241−5252

experiment where $KSiD_3$ was heated from 200 to 290 K (which is approximately 13 K below the phase transition seen in C_p measurements), and the spectrum at 290 K then showed the presence of 3% α-phase (Figure S3). Note that in the NPD experiment, performed upon heating, the α-phase was only recognized at temperatures above 300 K (cf. Figure 3a), in agreement with the phase transition temperature determined by the C_p measurement. Therefore, it has to be assumed that undercooled α-phase possesses a domain size too small for coherent scattering, i.e., crystallites are sub-Bragg (2−4 nm) sized and can only express short and medium range order. The β-to-α phase transition seen in diffraction and C_p experiments should then correspond to the sudden growth of α-phase domains. In the following we distinguish the occurrence of undercooled α-phase upon cooling and heating as remnant and premonitory, respectively.

Figure 9 shows selected QENS spectra for $ASiH_3$ (for a complete series, see ref 25). It is important to mention that the DCS instrument used for the QENS experiments senses dynamics in a temporal range 0.1−100 ps. Thus, only fast dynamics associated with the α-phase is probed. The β−α phase transition upon heating expresses itself with the sudden appearance of strong quasi-elastic scattering intensity, that is a broadening of the elastic line. This is seen between 300 and 305 K for $KSiH_3$ and 270 and 285 K for $RbSiH_3$, in agreement with the observations from the NPD and C_p measurements. Upon cooling, QENS spectra remain considerably broadened also at temperatures below the transition. This reflects the presence of remnant nonequilibrium α-phase domains, as established from the NMR experiments. As a matter of fact, a small broadening is also present in the spectra upon heating before the phase transition, which has to be attributed to the presence of premonitory α-phase. Thus, the QENS spectra mirror exactly the results from the ^2H NMR investigation.

In order to evaluate the QENS spectra, they were fitted with a function consisting of one elastic component together with two Lorentzian functions, $L_1(Q,w)$ and $L_2(Q,w)$. Of specific interest here is the width of the first Lorentzian, $\Gamma_1(Q)$, which carries information on the reorientational hopping motion of SiH_3^- as $\tau_1 = 2\hbar/\Gamma_1(Q)$, where τ_1 is a characteristic relaxation, also known as correlation, time. See Supporting Information, part 5, for details about the QENS analysis.

Figure 10 depicts Arrhenius plots of $\Gamma_1(Q)$ for the various temperature intervals—I: cooling until the phase transition; II: cooling after the phase transition; and III: heating until the phase transition. Tables 1 and 2 summarize relaxation times and activation energies, respectively. The Arrhenius dependence for "regular" α-$ASiH_3$ within interval I with activation energies of 39(1) and 33(1) meV for A = K and Rb, respectively, has been established earlier.[25] However, also $\Gamma_1(Q)$ in the intervals II and III, ascribed to remnant and premonitory α-phase, respectively, seem to follow an Arrhenius dependence, although less clear because of the lack of data and significantly larger error bars. The activation energies are increased, especially for $KSiH_3$. The relaxation times are 0.2−0.3 ps for the dynamics in regular α-$ASiH_3$ and increase by an order of magnitude for remnant and again another order of magnitude for premonitory α-phase. The increased reorientation barriers (activation energy) and decreased mobility (relaxation time) most likely correlate with the domain size of crystallites.

The geometry of the diffusional motion can be extracted from the elastic incoherent structure factor (EISF) which in

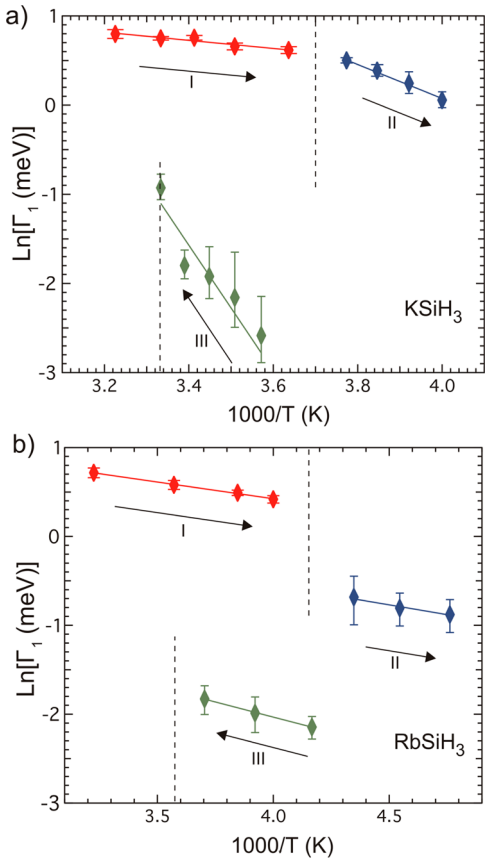

Figure 10. Arrhenius fits to the data of Γ_1 for $KSiH_3$ (a) and $RbSiH_3$ (b) when decreasing and increasing the temperature. The arrows indicate the temperature directions; broken horizontal lines indicate the phase transition temperatures according to C_p measurements (cf. Figure 7). The Roman numbers refer to the temperature intervals discussed in the text. High temperature data are taken from ref 25.

Table 1. Relaxation Times for $ASiH_3$

T_{down} (K)	$KSiH_3$ (ps)	T_{down} (K)	$RbSiH_3$ (ps)
310	0.22(5)	310	0.23(6)
300	0.23(2)	280	0.27(6)
293	0.24(3)	260	0.29(4)
285	0.25(4)	250	0.32(6)
275	0.26(4)	240	
270		230	3(2)
265	0.80(4)	220	3(1)
260	0.9(1)	210	3(1)
255	1.0(2)		
250	1.3(2)		
T_{up} (K)	$KSiH_3$ (ps)	T_{up} (K)	$RbSiH_3$ (ps)
280	17(14)	240	11(3)
285	11(11)	255	10(1)
290	9(5)	270	8(1)
295	8(3)		
300	3(1)		

Table 2. Activation Energies for α-$ASiH_3$

T range (K)	$KSiH_3$ (meV)	T range (K)	$RbSiH_3$ (meV)
310−275	39(1)	310−250	33(1)
265−250	164(33)	230−210	38(7)
280−300	606(102)	240−270	59(4)

DOI: 10.1021/acs.jpcc.6b12902
J. Phys. Chem. C 2017, 121, 5241−5252

turn is obtained from the Q dependence of the elastic part of the scattering function $A_0(Q)$; see ref 25 and Supporting Information, part 5, for details. Previously, a "24-sites" model was established which utilizes the 24 positions of a truncated cube as jump locations for H atoms. This model averages dynamics of a composite mechanism, comprising both reorientations of H atoms around the molecular C_3 axis and the 8-fold reorientation of this axis. To obtain a good fit, in addition, a fraction of 0.1 (10%) of H had to be considered as immobile. Figure 11 shows the experimental EISFs at various

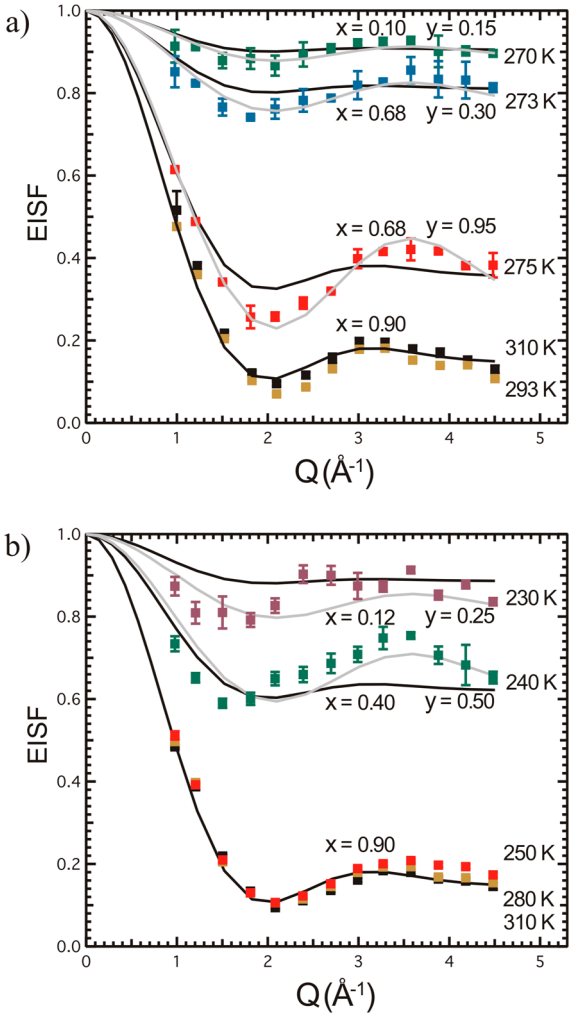

Figure 11. EISF during cooling over the phase transition for $KSiH_3$ (a) and $RbSiH_3$ (b) from data obtained using 2.5 Å neutrons (for 4.8 Å neutrons, see Supporting Information part 5, Figure S6). Two models are presented: the 24 sites model (blue line) and the C_3 model (gray line). The fractions of mobile hydrogen, contributing to an offset for the 24 sites model and the C_3 model, are shown by the values of x and y, respectively.

temperatures upon cooling, together with fits to two models. Certainly, the immobile fraction of H atoms increases abruptly when entering temperature interval II because of the formation of β-phase. Note that according to the C_p measurements, 275 and 240 K are very close to the phase transition for $KSiH_3$ and $RbSiH_3$, respectively. At the same time, the mechanism of dynamics in remnant α-phase seems to change from the "24-sites" model to a "C_3" model with only reorientation of H atoms around the molecular C_3 axis. This could be due to the lower temperature, leading to a "freezing out" of the component where the molecular axis is reoriented. More likely, however, is to assume a changed mechanism because of the small domain size of remnant α-phase. Note that the fitted values for the fraction of mobile H atoms (inserted in Figure 11) correlate with the fractions of remnant α-phase as established in the NMR experiments. No attempts were undertaken to extract and evaluate the EISF in the temperature interval of premonitory α-phase.

Dynamical Disorder and Thermodynamic Properties. The combination of a lone pair with hydridic hydrogen ligands is a peculiar feature of the silyl anion. Wolstenholme et al. have shown that for molecular systems "tetrahedral" (lone pair) and "inverted" (H_3) coordination of SiH_3^- by K^+ are essentially energetically degenerate.[53] Accordingly, the SiH_3^- ion can act as an ambidentate ligand which explains its orientational flexibility. At the same time, the high reorientational mobility and low activation energy of SiH_3^- in α-$ASiH_3$ imply that SiH_3^- ions are rather weakly coordinated by A^+ cations. The rotator state of α-$ASiH_3$ has to be associated with a high entropy, which in turn will affect the decomposition (hydrogen desorption) to ASi and H_2. The hydrogen release temperature is very similar for all three systems α-$ASiH_3$ (A = K, Rb, Cs), close to 410 K when referring to 0.1 MPa hydrogen equilibrium pressure.[23,24]

Interestingly, whereas $KSiH_3$ and $RbSiH_3$ indeed exhibit the expected low entropies of hydrogen desorption, ΔS_{des} [55−70 J/(K mol (H_2))], the one for $CsSiH_3$ is substantially higher [101 J/(K mol (H_2))].[24] Accordingly, the enthalpy of hydrogen desorption has to be larger for $CsSiH_3$, and the phenomenon has been explained by an enthalpy−entropy compensation effect. Although QENS measurements indicate a slightly changed dynamics for α-$CsSiH_3$ with a somewhat lower mobility of SiH_3^- (which has been attributed to a stronger interaction with the soft Cs^+ cations),[39] it appears unlikely that this should decisively influence ΔS_{des}. Alternatively, the enthalpy−entropy compensation could be explained by enthalpy and entropy changes in the precursor Zintl phases ASi. That is, if enthalpies of formation of ASi decreased and molar entropies increased when going from A = K to Cs, the same phenomenon would be observed. There are no thermodynamic data in the literature, but one could envision increasing disorder in the cubic phases ASi which are composed of Si_4^{4-} polyanions. These silicide polyanions are isoelectronic to P_4 (white phosphorus), which is a rotator phase.[5] The increasing unit cell volume from K to Cs may imply that Si_4^{4-} anions are coordinated less and less rigidly and that CsSi actually could correspond to a dynamically disordered high entropy phase at the temperatures applied for hydrogenation/dehydrogenation (373−473 K). In this case, the molar entropies for $CsSiH_3$ and CsSi will be similar and ΔS_{des} will essentially correspond to the gain of rotational and translational entropy of the released gaseous hydrogen [130 J/(K mol (H_2))].

IV. CONCLUSIONS

We investigated the transition of the silanides $KSiH_3$ and $RbSiH_3$ from their H-ordered low temperature (β) modifications into a rotator (α) phase near room temperature in which SiH_3^- moieties undergo rapid (subpicosecond) "close-to-isotropic" dynamics. This transition is associated with several peculiarities. First, we could confirm the presence of dynamics already in the low-temperature forms at temperatures above

DOI: 10.1021/acs.jpcc.6b12902
J. Phys. Chem. C 2017, 121, 5241−5252

200 K, as suggested earlier from FWS neutron scattering experiments.[39] A noticeable difference between $KSiH_3$ and $RbSiH_3$ is the occurrence of a triclinically distorted intermediate form for the latter prior to the phase transition. Second, there is a pronounced nonequilibrium behavior between the β and α phases. This is manifested in a large hysteresis of several tens of kelvin and the presence of undercooled α-phase upon cooling and heating. The latter phenomenon is attributed to a dependence of the transformation kinetics and/or relative stability of polymorphs on the size of α-phase domains. Undercooled α-phase is associated with small (2−4 nm) sized domains and it appears that the dynamics of SiH_3^- motion is changed to reduced dimensionality.

Evidently, the SiH_3^- anion is only loosely coordinated in an environment of alkali metal ions. The orientational flexibility can be attributed to the simultaneous presence of a lone pair and (weakly) hydridic hydrogen ligands, leading to an ambidentate coordination behavior toward cations A^+. The reorientational mobility of SiH_3^- affects the thermodynamic properties of the α-phase. With respect to hydrogen desorption, a simultaneous increase in the desorption enthalpy and entropy has been observed when going from A = K to Cs, leading to a similar release temperature of ca. 410 K (at 0.1 MPa H_2 pressure) for all three hydrides.[24] Rather to explain this enthalpy−entropy compensation effect by an increased stability and reduced SiH_3^- mobility within the silanide series, we attribute this phenomenon to enthalpy/entropy changes within the precursor Zintl phases ASi.

■ ASSOCIATED CONTENT

Supporting Information

The Supporting Information is available free of charge on the ACS Publications website at DOI: 10.1021/acs.jpcc.6b12902.

Figure S1: structural relationship between β-$KSiH_3$ and β-$RbSiH_3$; Figure S2: temperature-dependent heat capacity of $KSiD_3$ and $RbSiD_3$; Figure S3: static ^2H NMR spectrum of $KSiD_3$ recorded at 290 K upon heating from 200 K; compilations of NPD refinement results for $KSiD_3$; compilation of NPD refinement results for $RbSiD_3$; detailed description of the evaluation of C_p data; detailed description of the evaluation of QENS data (PDF)

■ AUTHOR INFORMATION

Corresponding Author

*E-mail: Ulrich.Haussermann@mmk.su.se (U.H.).

ORCID

Ulrich Häussermann: 0000-0003-2001-4410

Notes

The authors declare no competing financial interest.

■ ACKNOWLEDGMENTS

This work was supported by the Swedish Research Council (2010-4827, 2013-4690). We gratefully acknowledge the Science and Technology Facilities Council (STFC) for neutron beam time at the ISIS Facility, Rutherford Appleton Laboratory, and Dr. Ron Smith for assistance in performing the measurements. We further acknowledge the support of the National Institute of Standards and Technology (NIST), U.S. Department of Commerce, in providing the neutron research facilities used in this work. This work utilized facilities supported in part by the NSF under Agreement No. DMR-0944772. Certain commercial equipment, instruments, or materials are identified in this document. Such identification does not imply recommendation or endorsement by NIST, nor does it imply that the products identified are necessarily the best available for the purpose. M.E. acknowledges financial support from the Swedish Research Council (contract VR-NT 2014-4667), as well as NMR equipment Grants from the Knut and Alice Wallenberg Foundation, and the Swedish Research Council. Prof. W. Scherer, Augsburg University, is acknowledged for his interest in this work and for supporting the heat capacity measurement.

■ REFERENCES

(1) Clarke, J. B.; Hastie, J. W.; Kihlborg, L. H. E.; Metselaar, R.; Thackeray, M. M. Definitions of Terms Relating to Phase Transitions of the Solid State (IUPAC recommendations 1994). *Pure Appl. Chem.* **1994**, *66*, 577−594.

(2) Sherwood, J. N., Ed.; *The Plastically Crystalline State (Orientationally Disordered Crystals)*; Wiley: Chichester, 1979.

(3) Bonhoeffer, K. F.; Harteck, P. Über Para- und Orthowasserstoff. *Z. Phys. Chem. B-Chem. E* **1929**, *4*, 113−141.

(4) Press, W. Structure and Phase Transitions of Solid Heavy Methane (CD_4). *J. Chem. Phys.* **1972**, *56*, 2597−2609.

(5) Simon, A.; Borrmann, H.; Horakh, J. On the Polymorphism of White Phosphorus. *Chem. Ber.* **1997**, *130*, 1235−240.

(6) Heiney, P. A.; Fischer, J. E.; McGhie, A. R.; Romanow, W. J.; Denenstein, A. M.; McCauley, J. P., Jr.; Smith, A. B.; Cox, D. E. Orientational Ordering Transition in Solid C_{60}. *Phys. Rev. Lett.* **1991**, *66*, 2911−2914.

(7) Sirota, E. B.; King, H. E.; Singer, D. M.; Shao, H. H. Rotator Phases of the Normal Alkanes: An X-ray Scattering Study. *J. Chem. Phys.* **1993**, *98*, 5809−5824.

(8) Staveley, L. A. K. Phase Transitions in Plastic Crystals. *Annu. Rev. Phys. Chem.* **1962**, *13*, 351−368.

(9) Adebahr, J.; Grimsley, M.; Rocher, N. M.; MacFarlane, D. R.; Forsyth, M. Rotational and Translational Mobility of a Highly Plastic Salt: Dimethylpyrrolidinium Thiocyanate. *Solid State Ionics* **2008**, *178*, 1798−1803.

(10) Timmermans, J. Plastic Crystals: A Historical Review. *J. Phys. Chem. Solids* **1961**, *18*, 1−8.

(11) Eucken, A. Übergänge zwischen Ordnung und Unordnung in festen und flüssigen Phasen. *Z. Elektrochem.* **1939**, *45*, 126−144.

(12) Pauling, L. The Rotational Motion of Molecules in Crystals. *Phys. Rev.* **1930**, *36*, 430−442.

(13) Frenkel, J. Über die Drehung von Dipolmolekülen in festen Körpern. *Acta Physiochim. URSS* **1935**, *3*, 23−36.

(14) Krieger, T. J.; James, H. M. Successive Orientational Transitions in Crystals. *J. Chem. Phys.* **1954**, *22*, 796−814.

(15) Lyndenbell, R. M.; Michel, K. H. Translation-Rotation Coupling, Phase Transitions, and Elastic Phenomena in Orientationally Disordered Crystals. *Rev. Mod. Phys.* **1994**, *66*, 721−762.

(16) Smith, D. Hindered Rotation of the Ammonium Ion in the Solid State. *Chem. Rev.* **1994**, *94*, 1567−1584.

(17) Verdal, N.; Hartman, M. R.; Jenkins, T.; DeVries, D. J.; Rush, J. J.; Udovic, T. R. Reorientational Dynamics of $NaBH_4$ and KBH_4. *J. Phys. Chem. C* **2010**, *114*, 10027−10033.

(18) Remhof, A.; Lodziana, Z.; Martelli, P.; Friedrichs, O.; Züttel, A.; Skripov, A. V.; Embs, J. P.; Strässle, T. Rotational Motion of BH_4 Units in MBH_4 (M = Li, Na, K) from Quasielastic Neutron Scattering and Density Functional Calculations. *Phys. Rev. B: Condens. Matter Mater. Phys.* **2010**, *81*, 214304.

(19) Verdal, N.; Udovic, T. J.; Rush, J. J.; Stavila, V.; Wu, H.; Zhou, W.; Jenkins, T. Low-Temperature Tunneling and Rotational Dynamics of the Ammonium Cations in $(NH_4)_2B_{12}H_{12}$. *J. Chem. Phys.* **2011**, *135*, 094501.

(20) Ring, M. A.; Ritter, D. M. Crystal Structure of Potassium Silyl. *J. Phys. Chem.* **1961**, *65*, 182−183.

DOI: 10.1021/acs.jpcc.6b12902
J. Phys. Chem. C 2017, 121, 5241−5252

(21) Weiss, E.; Hencken, G.; Kuhr, H. Kristallstrukturen und kernmagnetische Breitlinienresonanz der Alkalisilyle SiH_3M (M = K, Rb, Cs). *Chem. Ber.* **1970**, *103*, 2868−2872.
(22) Mundt, O.; Becker, G.; Hartmann, H.-M.; Schwarz, W. Metallderivate von Molekülverbindungen. II. Darstellung und Struktur des β-Kaliumsilanids. *Z. Anorg. Allg. Chem.* **1989**, *572*, 75−88.
(23) Chotard, J.-N.; Tang, W. S.; Raybaud, P.; Janot, R. Potassium Silanide ($KSiH_3$): A Reversible Hydrogen Storage Material. *Chem. - Eur. J.* **2011**, *17*, 12302−12309.
(24) Tang, W. S.; Chotard, J.-N.; Raybaud, P.; Janot, R. Enthalpy−Entropy Compensation Effect in Hydrogen Storage Materials: Striking Example of Alkali Silanides $MSiH_3$ (M = K, Rb, Cs). *J. Phys. Chem. C* **2014**, *118*, 3409−3419.
(25) Österberg, C.; Fahlquist, H.; Häussermann, U.; Brown, C. M.; Udovic, T. J.; Karlsson, M. Dynamics of Pyramidal SiH_3^- Ions in $ASiH_3$ (A = K and Rb) Investigated with Quasielastic Neutron Scattering. *J. Phys. Chem. C* **2016**, *120*, 6369−6376.
(26) Larson, A. C.; Von Dreele, R. B. *General Structure Analysis System (GSAS)*; Los Alamos National Laboratory Report LAUR 86-748, 2004.
(27) Toby, B. H. EXPGUI, a Graphical User Interface for GSAS. *J. Appl. Crystallogr.* **2001**, *34*, 210−213.
(28) Azuah, R.; Kneller, L.; Qiu, Y.; Tregenna-Piggott, P. L. W.; Brown, C.; Copley, J.; Dimeo, R. DAVE: A Comprehensive Software Suite for the Reduction, Visualization, and Analysis of Low Energy Neutron Spectroscopic Data. *J. Res. Natl. Inst. Stand. Technol.* **2009**, *114*, 341−358.
(29) Bielecki, A.; Burum, D. P. Temperature Dependence of ^{207}Pb MAS Spectra of Solid Lead Nitrate. An Accurate, Sensitive Thermometer for Variable Temperature MAS. *J. Magn. Reson., Ser. A* **1995**, *116*, 215−220.
(30) Kranak, V. F.; Lin, Y.-C.; Karlsson, M.; Mink, J.; Norberg, S. T.; Häussermann, U. Structural and Vibrational Properties of Silyl (SiH_3^-) Anions in $KSiH_3$ and $RbSiH_3$: New Insight into Si−H Interactions. *Inorg. Chem.* **2015**, *54*, 2300−2309.
(31) Landon, G. J.; Ubbelohde, A. R. Volume Changes on Melting Ionic Crystals. *Trans. Faraday Soc.* **1956**, *52*, 647−651.
(32) Renaudin, G.; Gomes, S.; Hagemann, H.; Keller, L.; Yvon, K. Structural and Spectroscopic Studies on the Alkali Borohydrides MBH_4 (M = Na, K, Rb, Cs). *J. Alloys Compd.* **2004**, *375*, 98−106.
(33) Fischer, P.; Züttel, A. Order-Disorder Phase Transition in $NaBD_4$. *Mater. Sci. Forum* **2004**, *443*−*444*, 287−290.
(34) Note that the order−disorder transition in $LiBH_4$, leading to lithium superionic conduction in the hexagonal high temperature form, is accompanied with a slight contraction of the molar volume. Arnbjerg, L. M.; Ravnsbak, D. B.; Filinchuk, Y.; Vang, R. T.; Cerenius, Y.; Besenbacher, F.; Jorgensen, J.-E.; Jakobsen, H. J.; Jensen, T. R. Structure and Dynamics for $LiBH_4$−LiCl Solid Solutions. *Chem. Mater.* **2009**, *21*, 5772−5782.
(35) Bartlett, G.; Langmuir, I. The Crystal Structure of the Ammonium Halides Above and Below the Transition Temperature. *J. Am. Chem. Soc.* **1921**, *43*, 84−91.
(36) Levy, H. A.; Peterson, S. W. Neutron Diffraction Determination of the Crystal Structure of Ammonium Bromide in Four Phases. *J. Am. Chem. Soc.* **1953**, *75*, 1536−1542.
(37) Smirnov, L. S.; Natkaniec, I.; Savenko, B. N.; Kozlenko, D. P.; Kichanov, S. E.; Dlouha, M.; Vratislav, S.; Martinez-Sarrion, M. L.; Mestres, L.; Herraiz, M.; Shuvalov, L. A. Neutron Studies of the Structure and Dynamics of $Rb_{1-x}(NH_4)_xI$ Mixed Crystals. *Crystallogr. Rep.* **2004**, *49*, 653−659.
(38) Mink, J.; Lin, Y.-C.; Karlsson, M.; Österberg, C.; Udovic, T. J.; Fahlquist, H.; Häussermann, U. Vibrational Properties of β-KSiH3 and β-RbSiH3: A Combined Raman and Inelastic Neutron Scattering Study. *J. Raman Spectrosc.* **2017**, *48*, 284−291.
(39) Tang, W. S.; Dimitrievska, M.; Chotard, J.-N.; Janot, R.; Skripov, A. V.; Udovic, T. J. Structural and Dynamical Trends in Alkali-Metal Silanides Characterized by Neutron-Scattering Methods. *J. Phys. Chem. C* **2016**, *120*, 21218−21227.
(40) Sorai, M.; Suga, H.; Seki, S. Phase Transition in the Ammonium Bromide Crystal: The Thermal Motion of the Ammonium Ion. *Bull. Chem. Soc. Jpn.* **1965**, *38*, 1125−1136.
(41) Stephenson, C. C.; Karo, A. M. Heat Capacity of Deutero-Ammonium Bromide from 17° to 300 K. *J. Chem. Phys.* **1968**, *48*, 104−108.
(42) Pässler, R. Dispersion-Related Theory for Heat Capacities of Semiconductors. *Phys. Status Solidi B* **2007**, *244*, 4605−4623.
(43) Bartel, J. J.; Callanan, J. E.; Westrum, E. F. The Heat Capacity of NH_4Br from 265 to 550 K the II-to-I Transition. *J. Chem. Thermodyn.* **1980**, *12*, 753−760.
(44) Callanan, J. E.; Weir, R. D.; Staveley, L. A. The Thermodynamics of Mixed Crystals of Ammonium Chloride and Ammonium Bromide. I. The Heat Capacity from 8 to 476 K of an Approximately Equimolar Mixture. *Proc. R. Soc. London, Ser. A* **1980**, *372*, 489−496.
(45) Callanan, J. E.; Weir, R. D.; Staveley, L. A. The Thermodynamics of Mixed Crystals of Ammonium Chloride and Ammonium Bromide. II. An Analysis of the Heat Capacity of Ammonium Chloride, Ammonium Bromide, and an Approximately Equimolar Solid Solution of these Salts. *Proc. R. Soc. London, Ser. A* **1980**, *372*, 497−516.
(46) Stephenson, C. C.; Landers, L. A.; Cole, A. G. Rotation of the Ammonium Ion in the High Temperature Phase of Ammonium Iodide. *J. Chem. Phys.* **1952**, *20*, 1044.
(47) Lechner, R. E.; Badurek, G.; Dianoux, A. J.; Hervet, H.; Volino, F. On the Rotational Motion of the Ammonium Ion in the CsCl-type Phase of NH_4Br: Results from Quasielastic Neutron Scattering. *J. Chem. Phys.* **1980**, *73*, 934−939.
(48) Goyal, P. S.; Dasannacharya, B. A. Neutron Scattering from Ammonium Salts. II. Reorientational Motion of Ammonium Ions in Octahedral Environments. *J. Phys. C: Solid State Phys.* **1979**, *12*, 219−234.
(49) Westrum, E. F.; Justice, B. H. Molecular Freedom of the Ammonium Ion. Heat Capacity and Thermodynamic Properties of Ammonium Perchlorate from 5°−350 K. *J. Chem. Phys.* **1969**, *50*, 5083−5087.
(50) Herbstein, F. H. On the Mechanism of Some First-Order Enantiotropic Solid-State Phase Transitions: from Simon through Ubbelohde to Mnyukh. *Acta Crystallogr., Sect. B: Struct. Sci.* **2006**, *62*, 341−383.
(51) Spiess, H. W. Molecular Dynamics of Solid Polymers as Revealed by Deuteron NMR. *Colloid Polym. Sci.* **1983**, *261*, 193−209.
(52) Eckman, R. R.; Vega, A. J. Deuterium Solid-state NMR Study of the Dynamics of Molecules Sorbed by Zeolites. *J. Phys. Chem.* **1986**, *90*, 4679−4683.
(53) Wolstenholme, D. J.; Prince, P. D.; McGrady, G. S.; Landry, M. J.; Steed, J. W. Structure and Bonding of $KSiH_3$ and Its 18-Crown-6 Derivatives: Unusual Ambidentate Behavior of the SiH_3^- Anion. *Inorg. Chem.* **2011**, *50*, 11222−11227.

DOI: 10.1021/acs.jpcc.6b12902
J. Phys. Chem. C 2017, 121, 5241−5252